Extended Local Binary Pattern Features for Improving Settlement Type Classification of QuickBird Images

L. Mdakane and F. van den Bergh

Remote Sensing Research Unit, Meraka Institute
CSIR, PO Box 395, Pretoria
South Africa, 0001
Email: lmdakane@csir.co.za, fvdbergh@csir.co.za

Abstract—Despite the fact that image texture features extracted from high-resolution remotely sensed images over urban areas have demonstrated their ability to distinguish different classes, they are still far from being ideal. Multiresolution gray-scale and rotation invariant texture classification with Local Binary Patterns (LBPs) have proven to be a very powerful texture feature. In this paper we perform a study aiming to improve the performance of the automated classification of settlement type in high resolution imagery over urban areas. That is, we combined the LBP method based on recognising certain patterns, termed "uniform patterns" with the rotational invariant variance measure that characterises the contrast of the local image texture, then combined multiple operators for multiresolution analysis. The results showed that the joint distribution of these orthogonal measures improve performance over urban settlement type classification. This shows that variance measure (contrast) is an important property when classifying settlement types in urban areas.

I. Introduction

Rapid and massive growth of population and migration to urban areas results in a rapid and random spread of formal and informal physical infrastructure. Effective and regular monitoring of this spread of infrastructure is vital in delivering basic engineering services such as water, sewerage and solid waste removal, and providing essential services such as health and education. For a successful monitoring system, an effective detection method of this infrastructure is crucial. Traditional methods such as census, gathering demographic data, and mapping using samples are impractical and unsatisfactory for urban management [1]. However, using remote sensing tools an automated system can be used as a detection tool of physical infrastructure [2]. Using high resolution imagery (e.g., QuickBird, a high-resolution commercial earth observation satellite), texture feature algorithms have been shown to be effective in detecting and describing settlement types in urban areas [3].

In a study to compare texture algorithms in urban settlement classification, the Local Binary Pattern (LBP) texture feature algorithm proved to be most effective in classifying the low-income and informal settlement types [4]. A 2-D surface texture has two properties, spatial structure (pattern) and contrast ("amount of texture"). The LBP is simple to compute and by definition is gray scale invariant, that is, it neglects contrast properties which makes the LBP algorithm an excellent measure for spatial structures. However, due to viewing- and illumination-geometry effects, the LBP algorithm was shown to offer less than ideal generalization performance [3]. For settlement classification one would think neglecting the contrast measure would improve performance, but this does not appear to be the case for generalization performance. Contrast may have a significant effect in the classification of settlements.

Ojala [5] showed that combining spatial structure with the gray level contrast can improve performance in classifying texture features. In an attempt to improve performance for urban settlement classification, we apply this theory and evaluate the significance of contrast in urban settlement classification. The proposed algorithm uses the same rotational gray scale and rotational invariant LBP and combines it with a rotational invariant Variance measure which characterises the contrast.

In this paper (using Van den Bergh's [3] work on cross-date imagery for comparative results), we show that adding the rotational invariant variance measure to the gray-scale and rotational invariant LBP improves performance. The performance of the extended LBP algorithm then depends on the number of bins (features) used to calculate the Variance measures.

Section 2 briefly discusses prior and related urban settlements classification algorithms, and a brief derivation of the algorithms used. Section 3 discusses the experimental procedure i.e., extraction of the input images, LBP features extraction, extended LBP feature extraction and classification of the settlement types. Results with discussion are discussed in section 4, followed by conclusions in section 5.

II. Prior and Related work

Image texture analysis methods have been broadly divided into three categories: statistical methods (here a texture image is described by a collection of statistics of the selected feature, e.g., Co-occurence Matrix), model based methods (a texture

image is modeled as a probability model or as a linear combination of a set of basis functions, e.g., Wavelet transform [6] and Markov model [7]) and structural based methods (a texture image is viewed as consisting of many textural elements called texels, arranged according to some placement rules, e.g., Morphological Profiles [8]) [9].

In urban area images stuctural based methods have been shown to be successful in setting apart different settlement types [2]. The LBP (structural method) appeared to be most effective when compared to other known texture algorithms (e.g. Gray-level Co-occurrence Matrix (GLCM), Granulometrics and Discrete Wavelet Transform (DWT)) [4]. The LBP was used for cross-date Quickbird image (Soweto, located in Gauteng, South Africa as study area) urban settlement type classification and the results were not as impressive due to effects of varying viewing- and illumination geometry of satellite images [3].

The cross-date images study [3] involved the classification of two scenes of the same area acquired under different conditions. The images were acquired at different times of the year, which altered the orientation and length of the shadows. An ideal texture feature is one that is insensitive to such changes whilst being sensitive to settlement type. The addition of a contrast component to the LBP features does not directly effect the desired invariance to shadow orientation and length, but it is expected that the richer features will nevertheless improve settlement classification accuracy. The same data set (Soweto case study) will be used as basis for comparison with the extended LBP algorithm.

The extended LBP is a joint distribution of gray-scale and rotational invariant LBP with the rotational invariant Variance measure. We do not go into detail in the derivation of the algorithms but only report the equations used. The full derivations can be found in [5].

A. Gray-Scale and Rotational Invariant Local Binary Patterns

LBPs by definition are invariant with respect to any monotonic transformation of the gray scale. This is achieved by considering just the signs of differences instead of the exact values of the gray scale. Consider texture T

$$T \approx t(s(g_0 - g_c), s(g_1 - g_c), \ldots, s(g_{P-1} - g_c)) \quad (1)$$

in a local neighbourhood with gray levels of $P(P > 1)$ image pixels. Where $g_P(p = 0, \ldots, P-1)$ gray values, g_c being the centre gray value (see figure 2a), and

$$s(x) = \left\{ \begin{array}{l} 1, x \geq 0 \\ 0, x < 0 \end{array} \right. \quad (2)$$

the sign is 1 if positive and 0 if negative. The above is transformed into a unique P-bit pattern code by assigning binomial coefficient 2^P to each sign s$(g_P - g_c)$:

$$\text{LBP}_{P,R} = \sum_{p=0}^{P-1} s(g_P - g_c) 2^P \quad (3)$$

LBP features are then calculated using the rotational invariant LBP with "uniform patterns" (uniform circular structures, illustrated in figure 2b):

$$\text{LBP}_{P,R}^{\text{riu2}} = \left\{ \begin{array}{ll} \sum_{p=0}^{P-1} s(g_p - g_c) & \text{if } U(LBP_{P,R}) \leq 2 \\ P + 1 & \text{otherwise} \end{array} \right. \quad (4)$$

where

$$U(LBP_{P,R}) = \begin{array}{l} |s(g_{P-1} - g_c) - s(g_0 - g_c)| \\ + \sum_{p=0}^{P-1} |s(g_P - g_c) - s(g_{P-1} - g_c)|. \end{array} \quad (5)$$

U("pattern") is a uniformity measure, which corresponds to the number of spatial transitions in the "pattern" and superscript (riu2) is $r$otation $i$nvariant "$u$niform" binary patterns that have a U value of at most 2.

B. Rotational Invariant Variance Measures

Local gray level variance can be used as a contrast measure and can be derived as follows:

$$\text{VAR}_{P,R} = \frac{1}{P} \sum_{p=0}^{P-1} (g_p - \mu)^2, \text{where } \mu = \frac{1}{P} \sum_{p=0}^{P-1} g_p. \quad (6)$$

$\text{VAR}_{P,R}$ is invariant against shifts in gray scale and rotation along the circular neighbourhood.

To improve performance of the LBP we consider its joint distribution with the local variance denoted as $\text{LBP}_{P,R}^{\text{riu2}}/\text{VAR}_{P,R}$

III. Experiment

The data consisted of two QuickBird images over the Soweto area: one acquired on 2005-10-18 (early summer, rain season, called d1), and another on 2006-05-30 (early winter, called d2) [3]. QuickBird is a sun-synchronous polar-orbiting remote sensing satelitte with a panchromatic sensor with a 0.6 m ground sampling distance. This high resolution band, together with four multispectral bands at 2.4 m resolution, makes QuickBird ideal for urban monitoring. The study area contains a large variety of formal and informal settlements. Four settlement types are investigated: *formal suburbs(FS)*, *formal settlements with backyard shacks (FSB)*, *ordered informal settlements (OIS)*, and a *non-built-up (NBU)* class to represent vegetation and bare areas. Figure 1 provides some samples of what these settlement classes look like.

The experimental procedure was as follows:
1) *Extract input images*
   Two QuickBird images (Panchromatic images with a resolution of 0.6 m) over the same area at different times with different viewing- and illumination geometries were acquired. From each image, polygons containing examples of different settlement types were extracted, from which multiple non-overlapping examples of each type were extracted. From each polygon, square tiles (120 m × 120 m) from random locations entirely within the demarcated polygons were extracted. Tiles were

(a) formal settlement

(b) formal settlement with back-yard shacks
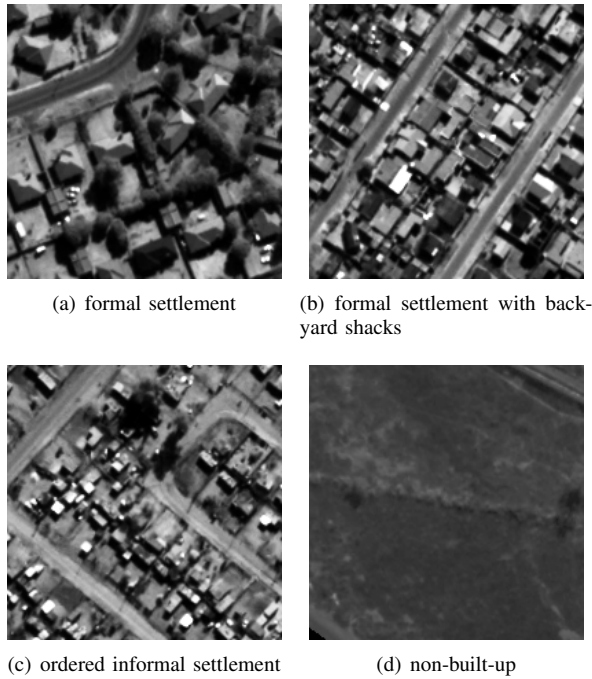
(c) ordered informal settlement

(d) non-built-up

Fig. 1. Examples of the settlements classes found in Soweto

paired, so that the same location is extracted from both dates (images) [3].

2) *Extract LBP features*

We construct regular circular neighbourhoods with P (P > 1) image pixels and radius R (R > 0), with the coordinates of the gray values g_P being $(-R \sin(2\pi p/P)), (R \cos(2\pi p/P))$ at $g_c(0,0)$. Gray values that do not fall exactly in the centre pixel are estimated by interpolation, see figure 2a. From the circular neighbourhood we measure the LBPs using equation 3. We construct a look-up table that contains all the uniformity measures corresponding to the number of image pixels used, see figure 2b. Using the look-up table LBPs with uniform patterns are extracted. Uniformity measures U with the value of at most 2 are stored as uniform patterns with bin labels ($0 \rightarrow$ P $- 1$) while the non-uniform patterns are stored as bin label (P $+ 1$), where bins $0 \rightarrow P - 1$ correspond to a texture feature from equation 5, see figures 2b and 2c.

3) *Extended LBP features extraction*

Using the circular neighbourhoods as mentioned above we calculate the Variance measure using equation 6. Since Variance measures have continuous outputs, quantization is needed. The bin breaks are constructed such that they are evenly spaced according to the variance percentiles, that is, by adding up all the feature distributions for every single model image in a total distribution and using R^1 we calculate the bin breaks for different number of bins ($3 \rightarrow 20$ bins in this case). We then constructed a simple 2D joint distribution histogram

[1]http://www.r-project.org/
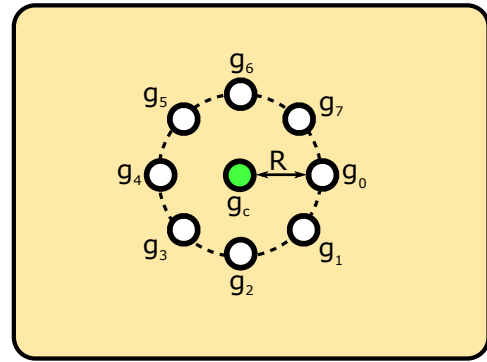
(a) Local circularly symmetric neighbourhood set (P = 8) of radius R, where g_1, g_3, g_5, g_7 are estimated by interpolation.
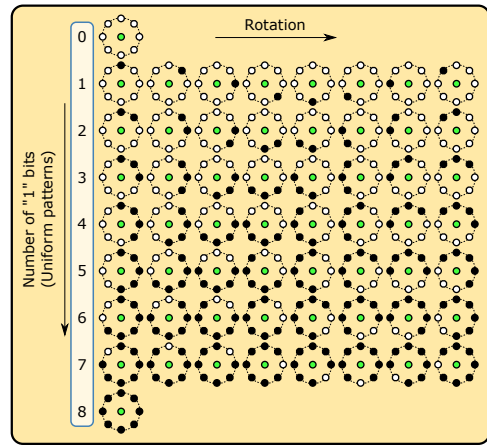
(b) The Look Up Table (LUT): To achieve rotation invariance the LUT is used to store all the posible the uniform patterns to their unique code i.e., for P = 8, nine "uniform" patterns with the numbers (0 − 8) corresponding to their unique $\mathrm{LBP}_{8,\mathrm{R}}^{\mathrm{riu2}}$ codes.
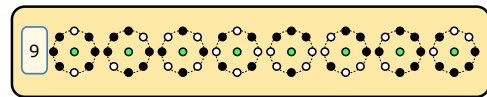
(c) A sample of nonuniform patterns, all of which are labeled as code 9.

Spot   Spot/flat   Line end   Edge   Corner
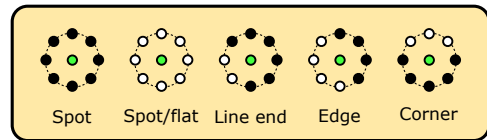
(d) Different texture primitives detected by the uniform patterns of LBP.

Fig. 2. Black and white circles correspond to bit values of 0 and 1 in the 8-bit pattern of the operator.

i.e LBP/VAR for each bin size for different P and R values. Multiresolution features are obtained by simply concatenating LBP features extracted at multiple radii (R parameter in equations 4 and 6).

4) *Training (Subset A) and Testing (Subset B)*

We determine the generalization performance for the different texture features algorithms by evaluating the
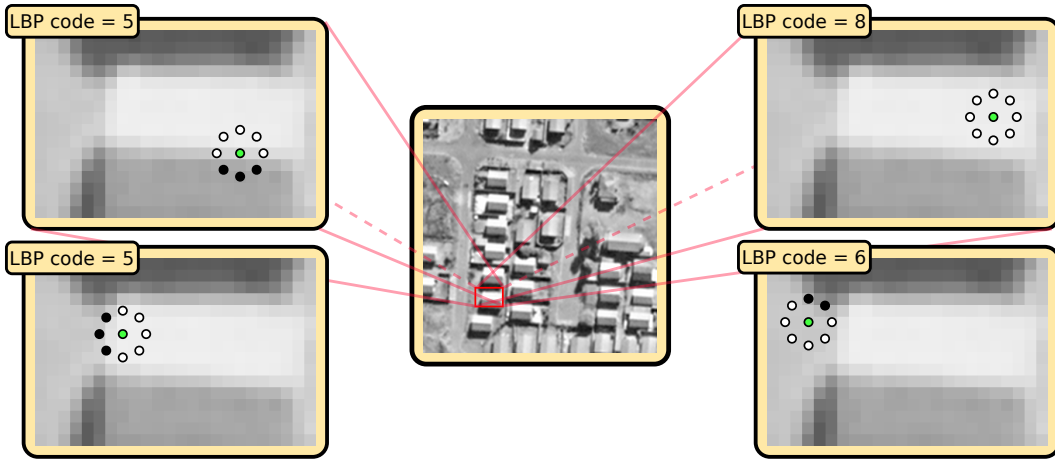
Fig. 3. Extraction of LBP features for P = 8.

performance of the Support Vector Machine (SVM) classifier over the six possible combinations (i.e. $A_{d1} \rightleftharpoons B_{d1}$, $A_{d2} \rightleftharpoons B_{d2}$, $A_{d1} \rightleftharpoons A_{d2}$, $A_{d1} \rightleftharpoons B_{d2}$, $B_{d1} \rightleftharpoons A_{d2}$, $B_{d1} \rightleftharpoons B_{d2}$ sets). We use Weka's[2] Sequential Minimal Optimization (SMO) algorithm for training the support vector classifier.

IV. RESULTS AND DISCUSSION

In a comparative study investigating the best algorithm for settlement classification, the LBP algorithm showed excellent performance [4]. However, it did not perform well when it was tested for cross-date imagery over the same area as the study mentioned above [3]. A study extending the LBP by adding variance measures (contrast properties) for texture classification, showed the extended LBP to be very powerful. We repeated the cross-date study for LBP [3] and implemented this new extended LBP with variance measures for urban settlement classification where the details are reported in table I.

TABLE I
THE NUMBER OF PATTERNS IN EACH CLASS, FOR EACH SUBSET.

	FS	FSB	OIS	NBU	Total
Subset A	557	2820	2059	1358	6794
Subset B	496	3915	1969	1180	7560

To obtain the standard deviations on various classification results, the following procedure was used to evaluate a given configuration using data sets X and Y (where $X = A_{d_1}$ and $Y = B_{d_1}$):

1. Train a support vector machine (SVM) using the whole of set X.
2. Partition set Y in 10 folds using stratified sampling to preserve related class frequency.
3. Evaluate the SVM (trained on X) on each of the 10 folds of Y, obtaining the one accuracy figure for each fold.

4. Exchange X and Y, and repeat 1–3.

This process, denoted by $X \rightleftharpoons Y$, produces 20 individual values for each accuracy metric, which were then used to calculate a mean and standard deviation for each metric. We distinguish between two classes of test, namely same-date (when both training and test sets are derived from the same-date satellite image) and cross-date (when two different satellite scenes were used). The difference in performance between these to classes highlights the degree to which a particular classifier is invariant to changes in shadow orientation and length.

From figure 4 it is clear that the extended LBP outperforms the LBP with no variance measures, achieving accuracies close to 95% and more for same-date experiments (e.g., $A_{d1} \rightleftharpoons B_{d1}$). Even for cross-date data set (i.e., $A_{d1} \rightleftharpoons B_{d2}, A_{d2} \rightleftharpoons B_{d1}$) the $\text{LBP}_{P,R}^{riu2}/\text{VAR}_{P,R}$ achieved close to 90%.

Overall performance is slightly improved by using the multiresolution features (see figure 4(a) and 4(b)), with the improvement being higher for $\text{LBP}_{8,1}^{riu2}/\text{VAR}_{8,1} + \text{LBP}_{16,2}^{riu2}/\text{VAR}_{16,2} + \text{LBP}_{24,3}^{riu2}/\text{VAR}_{24,3}$ achieving accuracies close to 95% on cross-date performance.

A more detailed comparison of the LBP and extended LBP with multiresolution is reported in table II, where we can clearly see the effects of adding the variance measures, bin sizes, and multiple resolutions. In all cases the $\text{LBP}_{P,R}^{riu2}/\text{VAR}_{P,R}$ features outperform the $\text{LBP}_{P,R}^{riu2}$ features. The performance drastically improves with the increase of bin sizes (3–6) but then fluctuates slightly as the number of bins are increased. Table II also shows a slight improvement from $\text{LBP}_{P,R}^{riu2}/\text{VAR}_{P,R}$ (8,1) to $\text{LBP}_{P,R}^{riu2}/\text{VAR}_{P,R}$ (8,1 + 16,2) but for $\text{LBP}_{P,R}^{riu2}/\text{VAR}_{P,R}$ (8,1 + 16,2 + 24,3) we observe slightly higher increase on accuracies. On all the figures in figure 4 we observed a peak around bin 7, and as the number of bins increased the performance was not meaningfully better. We then took bin 7 as the optimum number of bins and
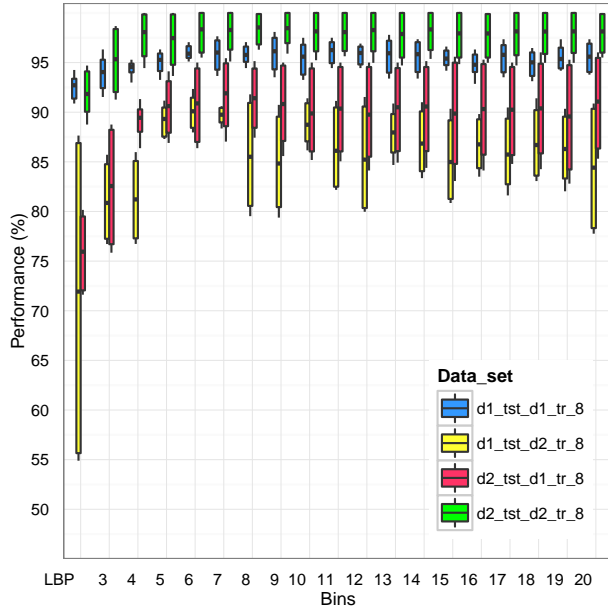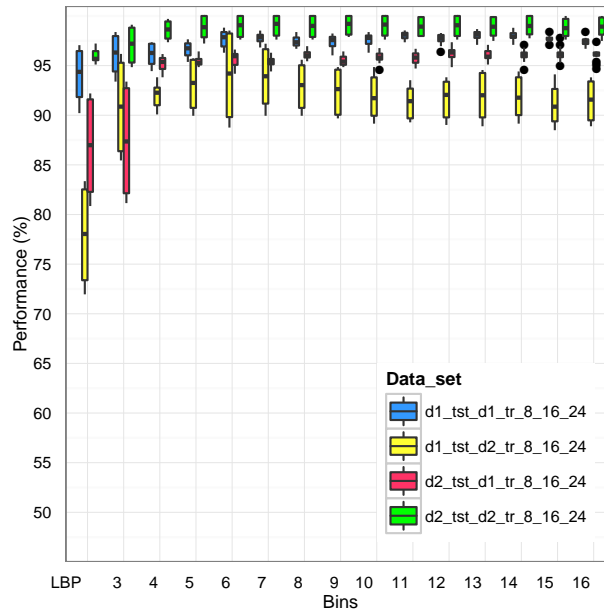
(a) P,R = 8,1
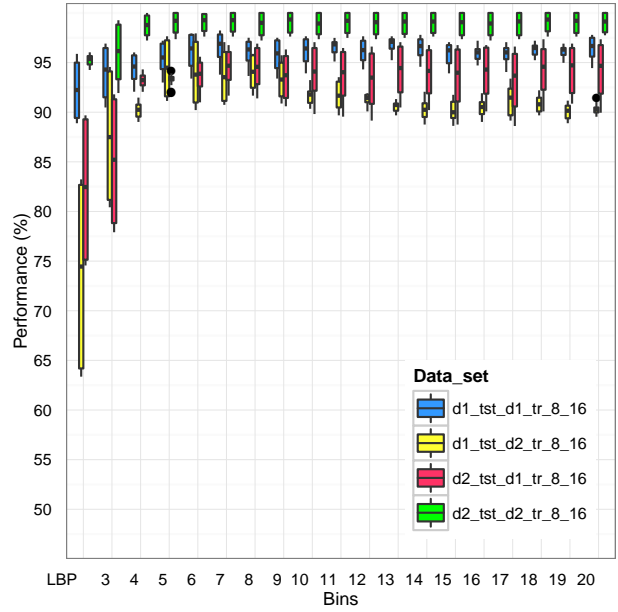
(b) P,R = 8,1+16,2

(c) P,R = 8,1+16,2+24,3

Fig. 4. Boxplots showing the overall performance(%) for $\mathrm{LBP}_{\mathrm{P,R}}^{\mathrm{riu2}}$ (LBP) and $\mathrm{LBP}_{\mathrm{P,R}}^{\mathrm{riu2}}/\mathrm{VAR}_{\mathrm{P,R}}$ (Bins) over same date and cross date imagery with multiresolution data sets (b) and (c).

investigated its accuracies in terms of per-class true positive (TP) rate (see table III). It is clear that the performance of the algorithm is depended on the settlement type, where we see that for formal settlements with backyard shacks (FSB) and non-built up (NBU) classes the TP values are much higher than those of formal settlements (FS) and ordered informal settlements (OIS) classes. The standard deviations for $A_{d1} \rightleftharpoons B_{d2}$ are high in all cases except for the NBU class where its standard deviation is high at $A_{d1} \rightleftharpoons A_{d2}$. Table III also reveals that 100% classification accuracy was attained for certain classes, which is too good to be true, and calls for further investigation of the algorithms with a larger data set.

Data set	$LBP^{riu2}_{P,R}$	$LBP^{riu2}_{8,1}/VAR_{8,1}$						
	P,R=8,1	3	6	8	10	12	14	16 (bins)
$A_{d1} \rightleftharpoons B_{d1}$	92.44 (1.185)	93.91 (1.507)	**95.99 (0.708)**	95.83 (0.814)	95.36 (1.658)	95.75 (0.932)	95.53 (1.537)	94.85 (1.096)
$A_{d1} \rightleftharpoons A_{d2}$	78.48 (3.610)	84.80 (5.675)	93.30 (0.864)	92.81 (1.982)	**93.89 (1.259)**	92.85 (1.891)	93.67 (1.453)	93.77 (1.552)
$A_{d1} \rightleftharpoons B_{d2}$	71.44 (15.932)	81.09 (3.921)	**90.06 (1.745)**	85.68 (5.302)	88.89 (1.909)	85.50 (5.274)	87.02 (3.251)	86.78 (2.553)
$B_{d1} \rightleftharpoons B_{d2}$	78.44 (14.956)	79.81 (1.549)	87.89 (6.545)	88.08 (6.537)	87.70 (7.207)	88.42 (6.309)	88.25 (6.814)	**88.58 (6.372)**
$A_{d2} \rightleftharpoons B_{d1}$	75.90 (3.820)	82.45 (5.730)	**90.79 (3.757)**	91.29 (3.227)	90.11 (4.327)	89.82 (4.720)	90.20 (4.571)	90.12 (4.843)
$A_{d2} \rightleftharpoons B_{d2}$	91.99 (2.149)	95.22 (3.294)	98.02 (2.055)	**98.33 (1.656)**	98.00 (2.053)	98.01 (2.027)	98.08 (1.946)	97.73 (2.257)
	P,R=8,1+16,2	$LBP^{riu2}_{8,1}/VAR_{8,1} + LBP^{riu2}_{16,2}/VAR_{16,2}$						
$A_{d1} \rightleftharpoons B_{d1}$	92.26 (2.831)	93.92 (2.624)	96.21 (1.625)	96.11 (1.141)	96.17 (1.358)	95.80 (1.033)	**96.51 (0.970)**	95.92 (0.715)
$A_{d1} \rightleftharpoons A_{d2}$	79.90 (6.158)	87.33 (5.677)	94.62 (1.088)	95.20 (0.699)	94.53 (1.148)	**95.89 (1.359)**	95.24 (1.277)	94.68 (1.445)
$A_{d1} \rightleftharpoons B_{d2}$	73.58 (9.492)	87.48 (6.647)	94.00 (3.186)	**94.01 (1.717)**	91.59 (0.761)	90.17 (0.987)	90.30 (0.962)	90.46 (0.800)
$B_{d1} \rightleftharpoons B_{d2}$	81.26 (12.159)	87.32 (2.321)	92.24 (2.311)	93.96 (1.207)	92.60 (2.442)	92.98 (2.227)	92.88 (2.608)	**93.99 (1.657)**
$A_{d2} \rightleftharpoons B_{d1}$	82.30 (7.146)	85.04 (6.422)	93.67 (1.498)	**94.51 (2.046)**	94.14 (2.461)	93.55 (2.978)	94.04 (2.370)	94.08 (2.505)
$A_{d2} \rightleftharpoons B_{d2}$	95.22 (0.544)	95.93 (2.999)	**98.99 (0.991)**	98.83 (1.178)	98.88 (1.143)	98.87 (1.111)	98.96 (1.070)	98.82 (1.204)
	P,R=8,1+16,2+24,3	$LBP^{riu2}_{8,1}/VAR_{8,1} + LBP^{riu2}_{16,2}/VAR_{16,2} + LBP^{riu2}_{24,3}/VAR_{24,3}$						
$A_{d1} \rightleftharpoons B_{d1}$	94.03 (2.553)	96.16 (1.956)	97.64 (0.826)	97.45 (0.540)	97.61 (0.559)	97.69 (0.280)	**97.96 (0.433)**	97.39 (0.420)
$A_{d1} \rightleftharpoons A_{d2}$	86.50 (0.658)	92.05 (2.222)	**94.21 (1.594)**	93.92 (0.699)	93.96 (0.548)	94.16 (0.673)	93.41 (0.361)	94.05 (0.785)
$A_{d1} \rightleftharpoons B_{d2}$	77.95 (4.768)	90.85 (4.571)	**94.00 (4.330)**	92.89 (2.253)	91.85 (2.182)	91.05 (1.842)	91.79 (2.069)	91.44 (2.051)
$B_{d1} \rightleftharpoons B_{d2}$	79.43 (1.220)	92.57 (0.624)	96.36 (1.469)	**97.23 (1.561)**	95.74 (0.640)	96.61 (0.693)	96.31 (0.553)	96.76 (0.645)
$A_{d2} \rightleftharpoons B_{d1}$	86.83 (4.893)	87.36 (5.396)	95.67 (0.708)	96.09 (0.430)	95.85 (0.543)	**96.16 (0.636)**	96.04 (0.541)	96.09 (0.545)
$A_{d2} \rightleftharpoons B_{d2}$	96.00 (0.693)	97.05 (1.797)	98.93 (1.069)	98.89 (1.083)	98.98 (1.027)	98.81 (0.904)	**98.99 (0.973)**	98.94 (0.972)

P,R	Bins	Data set	Overall Accuracy(%)	FS TP(%)	FSB TP(%)	OIS TP(%)	NBU TP(%)
8	7	$A_{d1} \rightleftharpoons B_{d1}$	95.782 (1.584)	87.170 (12.486)	96.330 (3.662)	96.060 (4.370)	100.00 (0.000)
		$A_{d1} \rightleftharpoons A_{d2}$	94.061 (0.885)	82.255 (20.412)	98.910 (0.485)	**86.870 (3.202)**	95.895 (4.277)
		$A_{d1} \rightleftharpoons B_{d2}$	89.658 (0.798)	76.580 (24.491)	97.615 (0.767)	65.725 (3.179)	99.900 (0.205)
		$B_{d1} \rightleftharpoons B_{d2}$	87.194 (7.331)	79.032 (20.347)	94.340 (3.273)	62.645 (37.457)	99.950 (0.154)
		$A_{d2} \rightleftharpoons B_{d1}$	91.641 (3.418)	79.412 (19.230)	95.675 (3.214)	82.310 (15.862)	97.905 (2.224)
		$A_{d2} \rightleftharpoons B_{d2}$	98.029 (2.050)	**96.817 (5.791)**	**99.985 (0.067)**	90.085 (10.299)	100.00 (0.000)
8+16	7	$A_{d1} \rightleftharpoons B_{d1}$	96.643 (1.343)	88.608 (10.171)	96.535 (3.387)	**99.380 (0.763)**	100.00 (0.000)
		$A_{d1} \rightleftharpoons A_{d2}$	95.244 (0.598)	**91.088 (12.430)**	99.175 (0.505)	85.685 (5.515)	96.220 (3.924)
		$A_{d1} \rightleftharpoons B_{d2}$	93.680 (2.471)	**83.285 (18.089)**	94.890 (1.558)	**87.390 (10.179)**	99.900 (0.205)
		$B_{d1} \rightleftharpoons B_{d2}$	92.882 (1.954)	82.093 (16.429)	96.550 (0.839)	84.915 (14.865)	99.950 (0.154)
		$A_{d2} \rightleftharpoons B_{d1}$	94.572 (1.676)	80.125 (18.795)	98.275 (1.166)	91.720 (7.774)	98.350 (1.913)
		$A_{d2} \rightleftharpoons B_{d2}$	**99.054 (0.987)**	96.537 (5.980)	99.850 (0.199)	97.255 (2.874)	100.00 (0.000)
8+16+24	7	$A_{d1} \rightleftharpoons B_{d1}$	**97.765 (0.476)**	**90.170 (10.245)**	**98.650 (1.402)**	99.080 (1.123)	100.00 (0.000)
		$A_{d1} \rightleftharpoons A_{d2}$	94.312 (1.702)	83.343 (17.415)	**99.890 (0.180)**	82.685 (14.843)	**97.100 (3.007)**
		$A_{d1} \rightleftharpoons B_{d2}$	**93.842 (2.980)**	76.737 (22.774)	**98.735 (1.323)**	85.930 (14.559)	**99.950 (0.154)**
		$B_{d1} \rightleftharpoons B_{d2}$	**96.107 (0.904)**	85.737 (18.993)	**97.970 (0.683)**	**95.630 (3.977)**	**99.975 (0.112)**
		$A_{d2} \rightleftharpoons B_{d1}$	**95.398 (0.482)**	83.028 (18.519)	**98.530 (1.249)**	**92.940 (2.316)**	**99.470 (0.983)**
		$A_{d2} \rightleftharpoons B_{d2}$	98.995 (1.047)	95.340 (7.982)	99.665 (0.367)	98.440 (1.693)	100.00 (0.000)

V. CONCLUSION

This paper presented a settlement classification experiment involving two scenes of the same area, acquired under different conditions, including seasonal changes in vegetation and the length and orientation of shadows cast by the buildings. The results indicate that adding the rotational invariant variance measure to the rotational and gray-scale invariant LBP does improve performance in classifying settlement types in urban areas. We can then conclude that contrast properties are significant in the task of classifying settlement type. Some differences remain between the classification performance in same-date experiments vs cross-date experiments; this is not entirely unexpected, since the addition of the contrast features is unlikely to provide robust invariance to the influence of

shadows. The good news, however, is that the gap between same-date and cross-date classification performance closed somewhat with the addition of contrast features, rather than widen.

Improvements to image features that result in better classifier generalization performance brings us one step closer towards operational implementation of a fully automated settlement type classification system. Once such a system has achieved adequate classification accuracy, the goal of automated change detection in urban areas is within reach.

REFERENCES

[1] D. Maktav, F. S. Erbek, and C. Jürgens, "Remote sensing of urban areas," *International Journal of Remote Sensing*, vol. 26, no. 4, pp. 655–659, 2005.

[2] J. Benediktsson, M. Pesaresi, and K. Amason, "Classification and feature extraction for remote sensing images from urban areas based on morphological transformations," *Geoscience and Remote Sensing, IEEE Transactions on*, vol. 41, no. 9, pp. 1940–1949, 2003.

[3] F. van den Bergh, "The effects of viewing- and illumination geometry on settlement type classification of quickbird images," in *Geoscience and Remote Sensing Symposium (IGARSS), 2011 IEEE International*, July 2011, pp. 1425 –1428.

[4] L. Ella, F. van den Bergh, B. van Wyk, and M. van Wyk, "A comparison of texture feature algorithms for urban settlement classification," in *Geoscience and Remote Sensing Symposium, 2008. IGARSS 2008. IEEE International*, vol. 3. IEEE, 2008.

[5] T. Ojala, M. Pietikainen, and T. Maenpaa, "Multiresolution gray-scale and rotation invariant texture classification with local binary patterns," *Pattern Analysis and Machine Intelligence, IEEE Transactions on*, vol. 24, no. 7, pp. 971 –987, July 2002.

[6] S. Arivazhagan and L. Ganesan, "Texture classification using wavelet transform," *Pattern Recognition Letters*, vol. 24, no. 910, pp. 1513 – 1521, 2003. [Online]. Available: http://www.sciencedirect.com/science/article/pii/S0167865502003902

[7] G. Rellier, X. Descombes, F. Falzon, and J. Zerubia, "Texture feature analysis using a Gauss-Markov model in hyperspectral image classification," *Geoscience and Remote Sensing, IEEE Transactions on*, vol. 42, no. 7, pp. 1543–1551, 2004.

[8] M. Pesaresi and J. Benediktsson, "A new approach for the morphological segmentation of high-resolution satellite imagery," *Geoscience and Remote Sensing, IEEE Transactions on*, vol. 39, no. 2, pp. 309–320, 2001.

[9] J. Zhang and T. Tan, "Brief review of invariant texture analysis methods," *Pattern Recognition*, vol. 35, no. 3, pp. 735–747, 2002.